Measuring the local Dark Matter density in the laboratory

Bradley J. Kavanagh[*]

*Instituto de Física de Cantabria (IFCA, UC-CSIC), Av. de Los Castros s/n, 39005 Santander, Spain and
Gravitation Astroparticle Physics Amsterdam (GRAPPA),
Institute for Theoretical Physics Amsterdam and Delta Institute for Theoretical Physics,
University of Amsterdam, Science Park 904, 1098 XH Amsterdam, The Netherlands*

Timon Emken[†] and Riccardo Catena[‡]
*Chalmers University of Technology,
Department of Physics,
SE-412 96 Göteborg, Sweden*
(Dated: April 3, 2020)

Despite strong evidence for the existence of large amounts of dark matter (DM) in our Universe, there is no direct indication of its presence in our own solar system. All estimates of the local DM density, crucial for all direct DM searches, rely on extrapolating estimates on much larger scales. We demonstrate for the first time the possibility of measuring the local DM density with a direct detection experiment. It relies on the assumption that incoming DM particles frequently scatter on terrestrial nuclei prior to detection, inducing an additional time-dependence of the signal. We show that for sub-GeV DM, with a spin-independent DM-proton cross section $\sim 10^{-32}\,\mathrm{cm}^2$, future direct detection experiments should be able to reconstruct the local DM density with 20% uncertainty.

Introduction.— A self-gravitating fluid that does not emit or absorb radiation at any observable wavelength, Dark Matter (DM) is the only coherent explanation for a number of otherwise anomalous phenomena [1, 2]. These range from the motions of stars in nearby dwarf spheroidal galaxies [3] to anisotropy patterns in the cosmic microwave background radiation [4]. There is also strong evidence for the presence of DM in the Milky Way, as inferred from kinematic measurements of stellar populations [5], microlensing events [6] and the dynamics of satellite galaxies [7].

While the evidence for the existence of DM in the Universe and in our own galaxy is compelling, there is no *direct* indication of the presence of DM within a sphere of radius about one parsec around the Sun [8]. More specifically, there is no astronomical tracer that can currently be used to directly probe the DM contribution to the Milky Way gravitational potential with sub-parsec resolution [9]. Consequently, any statement about the properties of the DM flux through our planet relies heavily on the extrapolation of DM density estimates performed on much larger scales. These estimates divide into two classes: 1) local methods based on the vertical motion of stellar populations [10–21]; 2) global methods relying on mass models for the Milky Way [22–30]. Each of these methods comes with its own limitations as well systematic and statistical errors [31–35]. Uncertainties inherent in these methods and the lack of direct astronomical measurements of the DM density at the Earth's location hinder the success of terrestrial experiments searching for Milky Way DM particles. This in particular applies to so-called direct detection experiments [36, 37]. These detectors search for non-relativistic DM-nucleus scattering events in deep underground laboratories, with an expected event rate depending on both the local DM density and the DM-nucleus scattering cross section.

Here, we explore a radically new approach to the problem of finding the local DM density at the Earth's location. We propose to exploit the diurnal variation of the DM flux *after* Earth-crossing to *simultaneously* measure the local DM density ρ_χ and DM-nucleus scattering cross section σ with future direct detection experiments. This diurnal variation arises from distortions in the DM distribution, due to interactions of DM particles in the Earth before they reach the detector. The amplitude of this modulation depends on the scattering cross section [38–41], as we will illustrate via Monte Carlo (MC) simulations, allowing us to break the well-known degeneracy between ρ_χ and σ. We show that using event timing information, combined with the energy spectrum of a hypothetical DM signal, can enable a measurement of the local DM density with future low-threshold experiments. We find that the precision of this measurement depends on where the detector is located on Earth, and can be smaller than about 20% for DM-proton scattering cross sections larger than 10^{-32} cm^2 and a DM particle mass around 200 MeV. Here, we focus on DM-nucleus scattering, but, if extended to DM-electron interactions, our method, which relies on existing experimental techniques, can be applied to DM candidates in the MeV-GeV range, covering a significant fraction of the parameter space of detectable DM candidates [42].

The simulation and statistics codes associated with this letter are publicly available at [43] and [44] respectively.

---
[*] kavanagh@ifca.unican.es
[†] emken@chalmers.se
[‡] catena@chalmers.se

Direct detection formalism.— The differential recoil rate for a DM particle of mass m_χ with a nucleus A of mass m_A can be written [45, 46]

$$\frac{\mathrm{d}R}{\mathrm{d}E_R} = \frac{\rho_\chi}{m_\chi m_A} \int_{v > v_{\min}} \mathrm{d}^3\mathbf{v} \; v \, f(\mathbf{v}) \frac{\mathrm{d}\sigma^{\mathrm{SI}}}{\mathrm{d}E_R} \,, \qquad (1)$$

with local DM density ρ_χ and local DM velocity distribution in the laboratory $f(\mathbf{v})$. Neglecting the effect of Earth scatterings, the usual choice for this distribution in the context of direct detection is the *standard halo model* (SHM) [45, 47, 48], a Maxwell-Boltzmann distribution in the galactic frame, truncated at the local galactic escape speed $v_{\mathrm{esc}} \approx 544\,\mathrm{km\,s^{-1}}$ [49, 50]. We integrate over $v > v_{\min}$, the minimum speed kinematically required to produce a nuclear recoil of energy E_R. It is a crucial feature of this work that for large enough cross sections both ρ_χ and $f(\mathbf{v})$ are modified by underground scatterings, thereby modifying the rate in Eq. (1). More details on this will be discussed in the next section.

We also assume standard spin-independent (SI) interactions for the differential scattering cross section,

$$\frac{\mathrm{d}\sigma^{\mathrm{SI}}}{\mathrm{d}E_R} = \frac{m_A \sigma_p^{\mathrm{SI}}}{2\mu_{\chi p}^2 v^2} A^2 F^2(E_R) \,. \qquad (2)$$

Here, σ_p^{SI} is the DM-proton cross section at zero momentum transfer and A the nucleus' mass number. We consider light DM, $m_\chi \ll m_A$, so we set the nuclear form factor $F^2(E_R) = 1$.

While we focus on spin-independent interactions as a proof of concept, similar analyses could just as well be performed for spin-dependent scattering [46], long-range interactions [51–53] or the broader class of effective field theory interactions [54–58]. Indeed, similar results should also apply for DM-electron scattering [59–61].

Earth scattering.— Above a certain DM-proton cross section $\sigma_p^{\mathrm{SI}} \gtrsim 10^{-37}\,\mathrm{cm^2}$, the probability for a DM particle to scatter on a terrestrial target becomes non-negligible. In this regime, underground scatterings prior to passing through the detector decelerate and deflect the incoming DM particles and thereby change the local DM density and distribution. These distortions grow with the cross section, and the signal thus depends non-linearly on σ_p^{SI}.

In the single-scattering regime of moderate cross sections, the impact of Earth scatterings on the local DM properties can be quantified analytically [40]. However, the precise contributions of multiple scatterings require the use of Monte Carlo (MC) simulations of underground DM particle trajectories [38, 39, 41], where we use the numerical tool DaMaSCUS [43][1]. The simulation details are described extensively in [41, 76], and we briefly review the essentials here.

Simulating an underground trajectory of a DM particle involves four random processes, namely the initial conditions of incoming particles, as well as the location, target, and scattering angle of the next scattering.

The initial positions of the DM particles are distributed uniformly throughout space, whereas the initial velocity distribution is given by the SHM, boosted into the Earth's rest frame. In order to determine if and where the DM particle scatters next along its path, we define the local mean free path,

$$\lambda^{-1}(\mathbf{x}) = \sum_i \lambda_i^{-1}(\mathbf{x}) \equiv \sum_i n_i(\mathbf{x})\sigma_i^{\mathrm{SI}}\,, \qquad (3)$$

where $n_i(\mathbf{x})$ is the local number density of isotope i, and σ_i^{SI} is the total DM-nucleus scattering cross section for that nucleus. The number densities depend on the Earth's mass density profile $\rho_\oplus(r)$, taken from the Preliminary Reference Earth Model (PREM) [77], and the relative nuclear abundances [78]. Once the location $\mathbf{x}$ of a scattering event is determined, the probability to scatter on a specific isotope j is given by $P_j(\mathbf{x}) = \lambda_j^{-1}(\mathbf{x}) \,/\, \lambda^{-1}(\mathbf{x})$. Finally, the differential cross section in Eq. (2) fixes the distribution of the scattering angle θ via its relation to the recoil energy, $E_R \propto (1 - \cos\theta)$.

The simulated system features an axial symmetry around the direction of the Earth's velocity $\mathbf{v}_\oplus$. This symmetry allows us to define the *isodetection angle* Θ [38, 39], the polar angle from the symmetry axis as illustrated in Fig. 1. The time-dependent local isodetection angle of a terrestrial observer at $\mathbf{x}_{\mathrm{obs}}$ reads

$$\Theta \equiv \angle(\mathbf{v}_\oplus, \mathbf{x}_{\mathrm{obs}}) = \arccos\left[\frac{\mathbf{v}_\oplus \cdot \mathbf{x}_{\mathrm{obs}}}{v_\oplus(r_\oplus - d)}\right]\,, \qquad (4)$$

where $r_\oplus \approx 6370\,\mathrm{km}$ is the Earth's radius, and $d \sim 1\,\mathrm{km}$ is the underground depth of the observer. It varies over a sidereal day, as described e.g. in App. A of [41].

To extract local estimates based on the MC simulations, we define isodetection rings of finite size $\Delta\Theta = 5°$. By counting the particles passing through each isodetection ring, we obtain an MC estimation of the local DM density $\hat{\rho}_\chi$. By recording their speeds, we obtain a (weighted) histogram estimate of the local speed distribution $\hat{f}(v, \Theta)$ [41]. Finally, these estimates are used to determine the local nuclear recoil spectrum expected for a given value of Θ via Eq. (1). We performed a grid of 36 MC simulations and evaluated the nuclear recoil spectra for DM parameters in the ranges $m_\chi \in [0.1, 0.5]\,\mathrm{GeV}$ and $\sigma_p^{\mathrm{SI}} = [10^{-38}, 10^{-30}]\,\mathrm{cm^2}$, accounting for the crucial impact of Earth scatterings.

Extracting the local DM density from data.— We express the sensitivity of direct detection experiments to the local DM density in terms of contours of constant p-value. We can then reject a point $\boldsymbol{\theta} = (\sigma_p^{\mathrm{SI}}, \rho_\chi)$ on these contours in favour of the alternative, benchmark point $\boldsymbol{\theta}' = (\sigma_p^{\mathrm{SI}\prime}, \rho_\chi')$ with a statistical significance of $\Phi^{-1}(1-p)$, where Φ is the standard normal distribution. For the local DM density, we assume $\rho_\chi' = 0.4\,\mathrm{GeV\,cm^{-3}}$, while for the

---

[1] Similar MC simulations have been used to study the sensitivity of terrestrial experiments to strongly interacting DM [63–68]. However, a number of analytic approximations have also been applied in this context [62, 69–75].
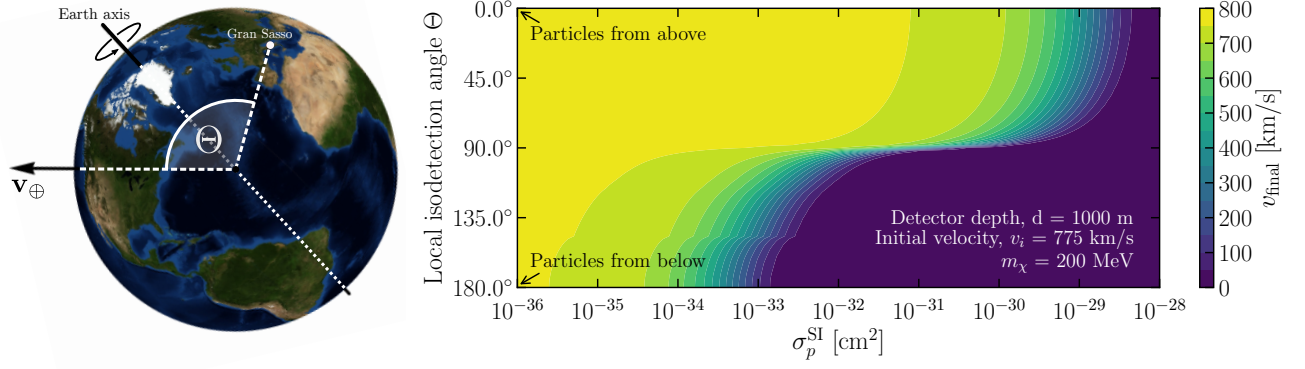
FIG. 1. **Left:** Visualization of the local isodetection angle defined in Eq. (4) at LNGS and a specific moment in time. **Right:** Final velocity of DM particles as a function of isodetection angle and DM-proton cross section σ_p^{SI}. For illustration only, we assume straight-line trajectories of DM particles [62] with initial speed $v_\oplus + v_{\mathrm{esc}} \approx 775\,\mathrm{km/s}$, travelling in the mean direction of the DM flux $-\mathbf{v}_\oplus$ (left-to-right in the left panel).

DM-proton scattering cross section we focus on 11 benchmark points, $\sigma_p^{\mathrm{SI}\prime}$, in the range $10^{-36}\,\mathrm{cm}^2$ - $10^{-30}\,\mathrm{cm}^2$.

We calculate such p-value contours by using $t_{\boldsymbol{\theta}} = -2\ln\lambda(\boldsymbol{\theta})$ as a test statistic, where $\lambda(\boldsymbol{\theta})$ is the profile likelihood ratio, defined in Eq. (7) of [79]. We account for the unknown DM mass by maximising the likelihood (at fixed $\boldsymbol{\theta}$) with respect to $m_\chi \in [0.1, 0.5]\,\mathrm{GeV}$. The p-value calculation requires the probability density function (pdf) of $t_{\boldsymbol{\theta}}$ under the assumption that the true model parameters are $\boldsymbol{\theta}$ or $\boldsymbol{\theta}'$. We denote these pdfs by $f(t_{\boldsymbol{\theta}}|\boldsymbol{\theta})$ and $f(t_{\boldsymbol{\theta}}|\boldsymbol{\theta}')$, respectively. Following [79], we approximate $f(t_{\boldsymbol{\theta}}|\boldsymbol{\theta})$ as a chi-square distribution with $k = 2$ degrees of freedom and $f(t_{\boldsymbol{\theta}}|\boldsymbol{\theta}')$ as a non-central chi-square distribution with the same number of degrees of freedom [79] and non-centrality parameter $\Lambda = -2\ln\lambda(\boldsymbol{\theta})$. Here, we restrict ourselves to "Asimov data", defined as the hypothetical dataset such that the maximum likelihood estimator, $\hat{\boldsymbol{\theta}}$, and benchmark point, $\boldsymbol{\theta}'$, coincide. The p-value for rejecting the hypothesised point $\boldsymbol{\theta}$ in favour of $\boldsymbol{\theta}'$ is then given by

$$p = \int_{t_{\boldsymbol{\theta}} > t_{\mathrm{med}}} \mathrm{d}t_{\boldsymbol{\theta}} f(t_{\boldsymbol{\theta}}|\boldsymbol{\theta}), \tag{5}$$

where t_{med} is the median of $f(t_{\boldsymbol{\theta}}|\boldsymbol{\theta}')$.

The profile likelihood ratio, $\lambda(\boldsymbol{\theta})$, depends on the expected number of nuclear recoils from DM signal and background events in the i-th energy bin and in the j-th time bin, s_{ij} and b_{ij}, respectively (see Eq. (7) in [79]). We calculate s_{ij}, $i = 1, \ldots, N$, $j = 1, \ldots, M$, by integrating Eq. (1) over $N = 12$ ($M = 12$) energy (time) bins of equal size. Motivated by existing experiments [80, 81], we assume a germanium detector, with a Gaussian energy resolution of 25 eV, a 30 day exposure with a target mass of 35 g, and perfect detection efficiency. The energy bins cover the energy interval that extends from the assumed experimental threshold, 100 eV, to a maximum energy of 1 keV. The time bins span 30 days, starting from January the 1st, 2020. We calculate b_{ij} as-

suming an energy- and time-independent background of 10 events/keV/kg/day. Finally, we assume a detector at a depth of $d = 1000\,\mathrm{m}$ underground.

Results.— The projected $p = 0.05$ contours in the $(\sigma_p^{\mathrm{SI}}, \rho_\chi)$-plane are shown in Fig. 2. The upper (lower) panel shows reconstructions of ρ_χ for a hypothetical direct detection experiment in the Northern (Southern) Hemisphere. We specify the experiments' locations by fixing their latitudes to the coordinates of the Laboratori Nazionali del Gran Sasso (LNGS) at 46°N and the Stawell Underground Physics Laboratory (SUPL) at 37°S respectively [82, 83].

We show as dashed, magenta contours our results taking only the recoil energies of the observed signal events into account, assuming no knowledge of their timing information. These contours demonstrate the strong degeneracy between σ_p^{SI} and ρ_χ, which can clearly not be broken by the energy data alone.

In contrast, keeping track of the signals' timing and accounting for their modulation signature caused by underground scatterings improves the situation drastically, as can be seen in the solid, blue contours of Fig. 2. In the case of the Northern experiment and cross sections above about $10^{-34}\,\mathrm{cm}^2$, we find that the degeneracy between DM density and scattering cross section starts to become weaker. For higher values of the benchmark cross sections, the true local DM density (as well as the cross section itself) can be reconstructed with higher and higher precision. For example, for $\sigma_p^{\mathrm{SI}} = 10^{-32}\,\mathrm{cm}^2$ ($\sigma_p^{\mathrm{SI}} = 10^{-31}\,\mathrm{cm}^2$) we could determine the local DM density to be $\rho_\chi = 0.40^{+0.11}_{-0.06}\,\mathrm{GeV\,cm}^{-3}$ ($\rho_\chi = 0.40^{+0.03}_{-0.03}\,\mathrm{GeV\,cm}^{-3}$) at 95% CL.

The development of the projected contours for an experiment at SUPL (lower panel) shows a more irregular evolution. While the ability to disentangle ρ_χ and σ_p^{SI} improves around cross sections of $\sim 10^{-34}\,\mathrm{cm}^2$, similarly to the Northern Hemisphere, the degeneracy is restored in an intermediate cross section regime around
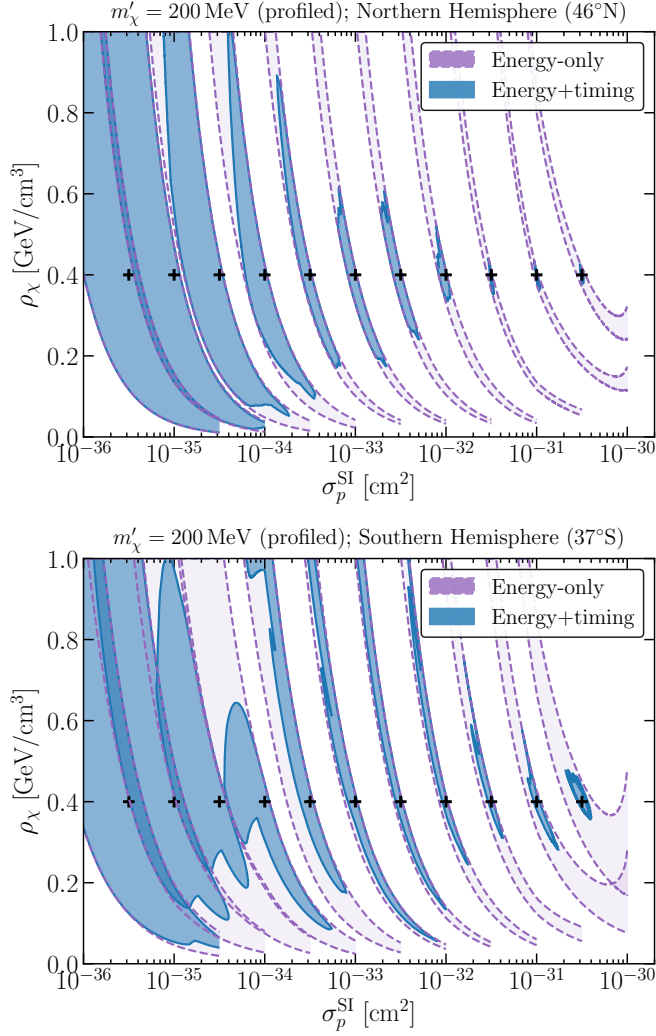
FIG. 2. Projected 95% CL contours using energy information only (dashed magenta) and using both energy and timing of events (solid blue). **Top:** detector in the Northern Hemisphere at LNGS. **Bottom:** detector in the Southern Hemisphere at SUPL.

$\sim 10^{-33} - 10^{-32}\,\mathrm{cm^2}$, and the precise reconstruction of the local DM density seems to be possible only at larger values of σ_p^{SI}. In addition, the contours assume a peculiar, unexpected shape, especially at the benchmark point $\sigma_p^{\mathrm{SI}} = 10^{-34}\,\mathrm{cm^2}$, which we investigate further below.

Discussion. — From these results, the necessity of timing information is obvious. Without time-tagging, it is always possible to reabsorb a change of the local DM density into a re-scaling of the cross section such that the overall normalisation $\rho_\chi \times \sigma_p^{\mathrm{SI}}$ remains constant. The time-dependence of the local DM distribution in the laboratory, caused by underground scatterings, introduces an additional dependence of the signal on σ_p^{SI}. Since this dependence manifests itself through a diurnal modulation signature, knowledge of the timing of the events is the key to disentangling the local DM density and the cross

section.

Contrary to our intuition[2], we find that experiments in the Northern Hemisphere are better suited to measuring the local DM density. For an experiment located at e.g. LNGS, $\Theta(t)$ varies in the range $[4°, 84°]$, so the bulk of the incoming DM flux reaches the laboratory directly from above at a certain time of day, while it has to pass through a small fraction of Earth's mantle 12 hours after that. Therefore, the experiment switches continuously between being totally exposed to and partially shielded from incoming DM particles, as illustrated in the right panel of Fig. 1. Increasing the cross section increases the amplitude of this modulation, and the reconstruction of the local DM density improves steadily for stronger interactions.

However, in order to reach a direct detection experiment in the Southern Hemisphere, the majority of DM particles need to traverse large parts of the planet's mass throughout the day. An experiment at e.g. SUPL is always partially shielded from the DM flux, with $\Theta(t) \in [86°, 167°]$. For cross sections between $10^{-34}-10^{-32}$ cm^2, the stopping power of the Earth renders the majority of the DM wind undetectable. The subdominant, slower component, which arrives from the opposite direction passing the atmosphere and overburden only, is not yet affected (see again Fig. 1). In this regime, the modulation amplitude depends only very weakly on the cross section, meaning the degeneracy between ρ_χ and σ_p^{SI} is restored around these values. This demonstrates that the determining factor for reconstructing the DM density is not so much the diurnal modulation's amplitude, but rather its sensitivity to changes in the cross section.

We now turn to the peculiar contour shapes for certain benchmarks in the lower panel of Fig. 2. In Fig. 3, we focus on the benchmark point $\sigma_p^{\mathrm{SI}} = 10^{-34}$ cm^2 and an experiment in the Southern Hemisphere. The left panel shows the projected contour and best fit mass at each point in parameter space $(\sigma_p^{\mathrm{SI}}, \rho_\chi)$, while the right panel shows the log-likelihood across four fixed cross section slices (A–D). In each slice, the curved region where the log-likelihood peaks corresponds roughly to a region where the total number of signal events N_{sig} is constant. Increasing the DM mass from the benchmark value (white dashed line) leads to an exponential increase in the number of events above the experimental threshold, which must be compensated by a decrease in ρ_χ. Decreasing m_χ increases the number density of DM particles crossing the experiment, which must again be compensated by reducing ρ_χ.

Focusing on slice A, underestimating the true value of the scattering cross section would mean predicting fewer events and a lower modulation amplitude. The former is compensated by a higher best-fit value of the local DM density, whereas the latter is compensated by an

---

[2] Detectors in the Southern Hemisphere are generally more sensitive to diurnal modulations caused by Earth scattering [39, 41].
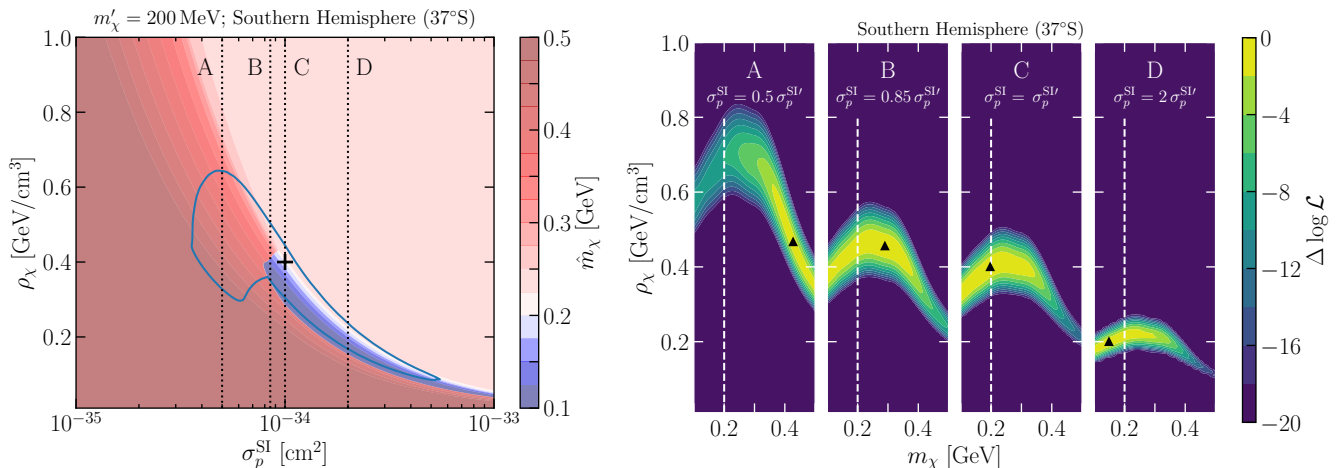
FIG. 3. **Left:** Projected 95% CL contour for a single benchmark (black cross), assuming a detector in the Southern Hemisphere. The colored shading shows the best fit DM mass at each point. **Right:** Log-likelihood contours in (m_χ, ρ_χ) for 4 fixed cross section slices through the parameter space, labelled A–D in the left panel. Vertical dashed lines show the benchmark mass $m'_\chi = 200\,\mathrm{MeV}$. The log-likelihood is shown relative to the best fit point in each slice (black triangle).

overestimate of m_χ, which in turn increases the Earth's stopping power.[3] At higher mass, the log-likelihood contours have a larger slope, meaning that in slice A, the uncertainties on ρ_χ are larger compared with slices B-D. In contrast, these unexpected 'hook'-shaped contours in $(\sigma_p^{\mathrm{SI}}, \rho_\chi)$ do not appear prominently in the Northern hemisphere, where the Earth-shielding effect is smaller for a given cross section, meaning the dependence of the modulation signal on m_χ is weaker.

Provided that DM-matter interactions are sufficiently strong for underground scatterings to occur frequently, the observed signals in direct detection experiments should show a diurnal modulation, which can be exploited to break the degeneracy between ρ_χ and σ_p^{SI}. We have explored this possibility for a number of benchmarks and scenarios using MC simulations. This is the first demonstration that it should be possible to measure the local Dark Matter density directly in the laboratory – especially in the Northern Hemisphere – and further

motivates the search for light, strongly-interacting DM with low-threshold detectors.

---

[3] At fixed cross-section, Earth stopping is more effective for DM closer to nuclear masses, due to the reduced kinematic mismatch.

[1] G. Bertone, D. Hooper, and J. Silk, Phys. Rept. **405**, 279 (2005), arXiv:hep-ph/0404175 [hep-ph].

[2] G. Bertone and D. Hooper, Rev. Mod. Phys. **90**, 045002 (2018), arXiv:1605.04909 [astro-ph.CO].

[3] E. L. Łokas, Mon. Not. R. Astron. Soc. **333**, 697 (2002).

[4] P. A. R. Ade *et al.* (Planck), Astron. Astrophys. **594**, A13 (2016), arXiv:1502.01589 [astro-ph.CO].

[5] A. G. A. Brown *et al.* (Gaia), Astron. Astrophys. **616**, A1 (2018), arXiv:1804.09365 [astro-ph.GA].

[6] M. Moniez, Gen. Rel. Grav. **42**, 2047 (2010), arXiv:1001.2707 [astro-ph.GA].

[7] T. Callingham, M. Cautun, A. J. Deason, C. S. Frenk, W. Wang, F. A. Gmez, R. J. J. Grand, F. Marinacci, and R. Pakmor, (2018), 10.1093/mnras/stz365, arXiv:1808.10456 [astro-ph.GA].

[8] S. Tremaine, SpringerLink , 37 (1990).

[9] N. P. Pitjev and E. V. Pitjeva, Astronomy Letters **39**, 141 (2013), arXiv:1306.5534 [astro-ph.EP].

[10] K. Kuijken and G. Gilmore, Mon. Not. Roy. Astron. Soc. **239**, 605 (1989).

[11] C. Moni Bidin, G. Carraro, R. A. Méndez, and R. Smith, Astrophys. J. **751**, 30 (2012), arXiv:1204.3924.

[12] J. Bovy and S. Tremaine, Astrophys. J. **756**, 89 (2012), arXiv:1205.4033 [astro-ph.GA].

[13] S. Garbari, C. Liu, J. I. Read, and G. Lake, MNRAS **425**, 1445 (2012), arXiv:1206.0015 [astro-ph.GA].

[14] M. C. Smith, S. H. Whiteoak, and N. W. Evans, Astrophys. J. **746**, 181 (2012), arXiv:1111.6920 [astro-ph.GA].

[15] L. Zhang, H.-W. Rix, G. van de Ven, J. Bovy, C. Liu, and G. Zhao, Astrophys. J. **772**, 108 (2013), arXiv:1209.0256.

[16] J. Bovy and H.-W. Rix, Astrophys. J. **779**, 115 (2013), arXiv:1309.0809 [astro-ph.GA].

[17] O. Bienaym *et al.*, Astron. Astrophys. **571**, A92 (2014), arXiv:1406.6896 [astro-ph.GA].

[18] C. F. McKee, A. Parravano, and D. J. Hollenbach, Astrophys. J. **814**, 13 (2015), arXiv:1509.05334 [astro-ph.GA].

[19] Q. Xia, C. Liu, S. Mao, Y. Song, L. Zhang, R. J. Long, Y. Zhang, Y. Hou, Y. Wang, and Y. Wu, Mon. Not. Roy. Astron. Soc. **458**, 3839 (2016), arXiv:1510.06810 [astro-ph.GA].

[20] S. Sivertsson, H. Silverwood, J. I. Read, G. Bertone, and P. Steger, Mon. Not. Roy. Astron. Soc. **478**, 1677 (2018), arXiv:1708.07836 [astro-ph.GA].

[21] J. Buch, S. C. J. Leung, and J. Fan, JCAP **1904**, 026 (2019), arXiv:1808.05603 [astro-ph.GA].

[22] P. Salucci, F. Nesti, G. Gentile, and C. F. Martins, Astron. Astrophys. **523**, A83 (2010), arXiv:1003.3101 [astro-ph.GA].

[23] R. Catena and P. Ullio, JCAP **1008**, 004 (2010), arXiv:0907.0018 [astro-ph.CO].

[24] M. Weber and W. de Boer, Astron. Astrophys. **509**, A25 (2010), arXiv:0910.4272 [astro-ph.CO].

[25] F. Iocco, M. Pato, G. Bertone, and P. Jetzer, JCAP **1111**, 029 (2011), arXiv:1107.5810 [astro-ph.GA].

[26] P. J. McMillan and J. J. Binney, MNRAS **402**, 934 (2010), arXiv:0907.4685.

[27] M. Pato, F. Iocco, and G. Bertone, JCAP **1512**, 001 (2015), arXiv:1504.06324 [astro-ph.GA].

[28] Y. Huang, X.-W. Liu, H.-B. Yuan, M.-S. Xiang, H.-W. Zhang, B.-Q. Chen, J.-J. Ren, C. Wang, Y. Zhang, Y.-H. Hou, Y.-F. Wang, and Z.-H. Cao, MNRAS **463**, 2623 (2016), arXiv:1604.01216.

[29] P. J. McMillan, MNRAS **465**, 76 (2017), arXiv:1608.00971.

[30] P. F. de Salas, K. Malhan, K. Freese, K. Hattori, and M. Valluri, "JCAP" **2019**, 037 (2019), arXiv:1906.06133 [astro-ph.GA].

[31] A. H. G. Peter, Phys. Rev. **D83**, 125029 (2011), arXiv:1103.5145 [astro-ph.CO].

[32] B. J. Kavanagh and A. M. Green, Phys. Rev. **D86**, 065027 (2012), arXiv:1207.2039 [astro-ph.CO].

[33] B. J. Kavanagh, Phys. Rev. **D89**, 085026 (2014), arXiv:1312.1852 [astro-ph.CO].

[34] B. J. Kavanagh and A. M. Green, Phys. Rev. Lett. **111**, 031302 (2013), arXiv:1303.6868 [astro-ph.CO].

[35] B. J. Kavanagh, M. Fornasa, and A. M. Green, Phys. Rev. **D91**, 103533 (2015), arXiv:1410.8051 [astro-ph.CO].

[36] A. Drukier and L. Stodolsky, Phys. Rev. D **30**, 2295 (1984).

[37] M. W. Goodman and E. Witten, Phys. Rev. D **31**, 3059 (1985).

[38] J. I. Collar and F. T. Avignone, III, Phys. Rev. **D47**, 5238 (1993).

[39] F. Hasenbalg, D. Abriola, F. T. Avignone, J. I. Collar, D. E. Di Gregorio, A. O. Gattone, H. Huck, D. Tomasi, and I. Urteaga, Phys. Rev. **D55**, 7350 (1997), arXiv:astro-ph/9702165 [astro-ph].

[40] B. J. Kavanagh, R. Catena, and C. Kouvaris, JCAP **1701**, 012 (2017), arXiv:1611.05453 [hep-ph].

[41] T. Emken and C. Kouvaris, JCAP **1710**, 031 (2017), arXiv:1706.02249 [hep-ph].

[42] G. Bertone and M. P. Tait, Tim, Nature **562**, 51 (2018), arXiv:1810.01668 [astro-ph.CO].

[43] T. Emken and C. Kouvaris, "Dark Matter Simulation Code for Underground Scatterings (DaMaSCUS) [Code, v1.1]," https://github.com/temken/damascus, DOI:10.5281/zenodo.3726878 (2017-2020).

[44] B. J. Kavanagh and R. Catena, "EarthScatterLikelihood [Code, v0.9]," https://github.com/bradkav/EarthScatterLikelihood, DOI:10.5281/zenodo.3725882 (2020).

[45] J. D. Lewin and P. F. Smith, Astropart. Phys. **6**, 87 (1996).

[46] D. G. Cerdeno and A. M. Green, "Direct detection of WIMPs," in *Particle Dark Matter: Observations, Models and Searches*, edited by G. Bertone (2010) pp. 347–369, arXiv:1002.1912 [astro-ph.CO].

[47] A. M. Green, Mod. Phys. Lett. **A27**, 1230004 (2012), arXiv:1112.0524 [astro-ph.CO].

[48] A. M. Green, J. Phys. **G44**, 084001 (2017), arXiv:1703.10102 [astro-ph.CO].

[49] M. C. Smith *et al.*, Mon. Not. Roy. Astron. Soc. **379**, 755 (2007), arXiv:astro-ph/0611671 [astro-ph].

[50] T. Piffl *et al.*, Astron. Astrophys. **562**, A91 (2014), arXiv:1309.4293 [astro-ph.GA].

[51] N. Fornengo, P. Panci, and M. Regis, Phys. Rev. **D84**, 115002 (2011), arXiv:1108.4661 [hep-ph].

[52] E. Del Nobile, C. Kouvaris, P. Panci, F. Sannino, and J. Virkajarvi, JCAP **1208**, 010 (2012), arXiv:1203.6652 [hep-ph].

[53] F. Kahlhoefer, S. Kulkarni, and S. Wild, JCAP **1711**, 016 (2017), arXiv:1707.08571 [hep-ph].

[54] J. Fan, M. Reece, and L.-T. Wang, JCAP **1011**, 042 (2010), arXiv:1008.1591 [hep-ph].

[55] A. L. Fitzpatrick, W. Haxton, E. Katz, N. Lubbers, and Y. Xu, JCAP **1302**, 004 (2013), arXiv:1203.3542 [hep-ph].

[56] M. Cirelli, E. Del Nobile, and P. Panci, JCAP **1310**, 019 (2013), arXiv:1307.5955 [hep-ph].

[57] E. Del Nobile, Phys. Rev. **D98**, 123003 (2018), arXiv:1806.01291 [hep-ph].

[58] R. Catena, K. Fridell, and M. B. Krauss, JHEP **08**, 030 (2019), arXiv:1907.02910 [hep-ph].

[59] R. Essig, J. Mardon, and T. Volansky, Phys. Rev. **D85**, 076007 (2012), arXiv:1108.5383 [hep-ph].

[60] R. Essig, M. Fernandez-Serra, J. Mardon, A. Soto, T. Volansky, and T.-T. Yu, JHEP **05**, 046 (2016), arXiv:1509.01598 [hep-ph].

[61] S. Derenzo, R. Essig, A. Massari, A. Soto, and T.-T. Yu, Phys. Rev. **D96**, 016026 (2017), arXiv:1607.01009 [hep-ph].

[62] B. J. Kavanagh, Phys. Rev. **D97**, 123013 (2018), arXiv:1712.04901 [hep-ph].

[63] G. Zaharijas and G. R. Farrar, Phys. Rev. **D72**, 083502 (2005), arXiv:astro-ph/0406531 [astro-ph].

[64] T. Emken, C. Kouvaris, and I. M. Shoemaker, Phys. Rev. **D96**, 015018 (2017), arXiv:1702.07750 [hep-ph].

[65] M. S. Mahdawi and G. R. Farrar, JCAP **1712**, 004 (2017), arXiv:1709.00430 [hep-ph].

[66] T. Emken and C. Kouvaris, Phys. Rev. **D97**, 115047 (2018), arXiv:1802.04764 [hep-ph].

[67] M. S. Mahdawi and G. R. Farrar, JCAP **1810**, 007 (2018), arXiv:1804.03073 [hep-ph].

[68] T. Emken, R. Essig, C. Kouvaris, and M. Sholapurkar, JCAP **1909**, 070 (2019), arXiv:1905.06348 [hep-ph].

[69] C. Kouvaris and I. M. Shoemaker, Phys. Rev. **D90**, 095011 (2014), arXiv:1405.1729 [hep-ph].

[70] C. Kouvaris, Phys. Rev. **D93**, 035023 (2016), arXiv:1509.08720 [hep-ph].

[71] J. H. Davis, Phys. Rev. Lett. **119**, 211302 (2017), arXiv:1708.01484 [hep-ph].

[72] D. Hooper and S. D. McDermott, Phys. Rev. **D97**, 115006 (2018), arXiv:1802.03025 [hep-ph].

[73] J. Bramante, B. Broerman, R. F. Lang, and N. Raj, Phys. Rev. **D98**, 083516 (2018), arXiv:1803.08044 [hep-ph].

[74] J. Bramante, B. Broerman, J. Kumar, R. F. Lang, M. Pospelov, and N. Raj, Phys. Rev. **D99**, 083010 (2019), arXiv:1812.09325 [hep-ph].

[75] J. Bramante, J. Kumar, and N. Raj, Phys. Rev. **D100**, 123016 (2019), arXiv:1910.05380 [hep-ph].

[76] T. Emken, *Dark Matter in the Earth and the Sun – Simulating Underground Scatterings for the Direct Detection of Low-Mass Dark Matter*, Ph.D. thesis, University of Southern Denmark, CP^3-Origins (2019), arXiv:1906.07541 [hep-ph].

[77] A. M. Dziewonski and D. L. Anderson, Phys. Earth Planet. Interiors **25**, 297 (1981).

[78] W. F. McDonough, Treatise on Geochemistry **2**, 568 (2003).

[79] G. Cowan, K. Cranmer, E. Gross, and O. Vitells, Eur. Phys. J. **C71**, 1554 (2011), [Erratum: Eur. Phys. J.C73,2501(2013)], arXiv:1007.1727 [physics.data-an].

[80] E. Armengaud *et al.* (EDELWEISS), Phys. Rev. **D99**, 082003 (2019), arXiv:1901.03588 [astro-ph.GA].

[81] Q. Arnaud *et al.* (EDELWEISS), (2020), arXiv:2003.01046 [astro-ph.GA].

[82] E. Bellotti, Nucl. Instrum. Meth. A **264**, 1 (1988).

[83] P. Urquijo, *Proceedings, Heavy Ion Accelerator Symposium on Fundamental and Applied Science (HIAS 2015): Canberra, Australia, September 14-18, 2015*, EPJ Web Conf. **123**, 04002 (2016), arXiv:1605.03299 [physics.ins-det].

[84] T. Oliphant, "NumPy: A guide to NumPy," USA: Trelgol Publishing (2006–), [Online; accessed 03/04/2020].

[85] E. Jones, T. Oliphant, P. Peterson, *et al.*, "SciPy: Open source scientific tools for Python," (2001–), [Online; accessed 03/04/2020].

[86] J. D. Hunter, Computing in Science & Engineering **9**, 90 (2007).